Preprint Cambridge Centre for Computational Chemical Engineering ISSN 1473 – 4273

# The polarisation of polycyclic aromatic hydrocarbons curved by pentagon incorporation: the role of the flexoelectric dipole

Jacob W. Martin [1], Radomir I. Slavchov [1], Edward K. Y. Yapp [2], Jethro Akroyd [1], Sebastian Mosbach [1] and Markus Kraft [1,2]

released: 21 August 2017

[1] Department of Chemical Engineering and Biotechnology
University of Cambridge
West Site, Philippa Fawcett Drive
Cambridge, CB3 0AS
United Kingdom
E-mail: mk306@cam.ac.uk

[2] School of Chemical and Biomedical Engineering
Nanyang Technological University
62 Nanyang Drive
Singapore 637459

Preprint No. 188

UNIVERSITY OF CAMBRIDGE

*Keywords:* curved polycyclic arene, fullerene-like hydrocarbon, buckybowls, carbon nanocone, flexoelectricity

**Edited by**
Computational Modelling Group
Department of Chemical Engineering and Biotechnology
University of Cambridge
West Site, Philippa Fawcett Drive
Cambridge, CB3 0AS
United Kingdom

**Fax:** + 44 (0)1223 334796
**E-Mail:** c4e@cam.ac.uk
**World Wide Web:** http://como.cheng.cam.ac.uk/

**Abstract**

Curvature in polyaromatic hydrocarbons (PAHs), due to pentagon integration, produces a dipole moment that contributes significantly to self-assembly processes and adsorption at the surface of carbon materials containing curved structures. This work presents electronic structure calculations of the dipole moment for 18 different curved PAH molecules for various numbers of pentagons and total number of aromatic rings. A significant dipole moment was found that depends strongly on the number of aromatic rings (4–6.5 debye for ring count 10–20). The main cause for the dipole is shown to be the $\pi$-electron flexoelectric effect. An atom-centred partial charge representation of the charge distribution in these molecules is insufficient to correctly describe their electrostatic potential; distributed multipoles were instead required.

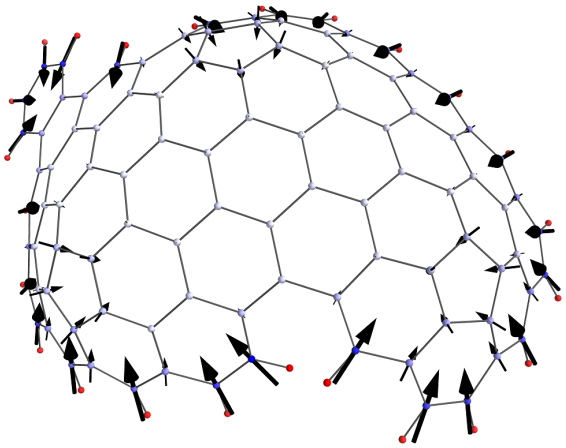

## Highlights

- The dipole moment was calculated for a range of curved polycyclic aromatic hydrocarbons.
- The $\pi$-electronic flexoelectric effect is the main contributor to the dipole moment.
- Atom-centred point charge models of curved arenes are inadequate; point dipoles have to be accounted for.

# Contents

# 1 Introduction

Fullerene-like curved polyaromatic hydrocarbon (PAH) fragments are known to be important intermediaries in combustion synthesis of fullerenes and have been suggested to make up the nanostructure of soot and activated carbon [23, 48, 62, 67]. Fullerenes can be formed in flames at low pressures [42] and curved fragments, such as corannulene (Figure 1, structure **1a**), have been extracted from soot [30]. In our recent transmission electron microscopy (TEM) studies of soot we have observed curved and completely closed graphitic structures (fringes) [7]. TEM fringes also were observed in synthetic soot made of hexabenzocoronene, a flat PAH, but, the fringes from natural soot are of apparently higher curvature [53]. Our recent kinetic Monte Carlo simulation of combustion synthesis of PAH with curvature integration showed degrees of curvature similar to the one observed with TEM images, with curved PAH containing one to three pentagons [67]. Alongside soot, curved arenes have been shown to be present in activated carbon imaged using aberration-corrected TEM [23]. In glassy carbon [22], closed fringes resembling icosahedral fullerenes have also been observed. These fullerene-like fragments have been suggested to provide the large surface area-to-volume ratio of activated carbon [54, 55]. A potential formation mechanism has been experimentally investigated where addition of methyl radicals to a pentagonal ring leads to the formation of corannulene, the $C_1/C_2$ formation mechanism [64]. For larger PAH molecules integration of pentagons through pyrolysis of a bay-site or oxidation of a zigzag edge has been suggested [48, 62, 69].

The integration of curvature into a hexagonal carbon lattice through a pentagonal point defect gives rise to a considerable molecular dipole moment. For example, corannulene (the first curved PAH to be synthesised [31]) was found experimentally to contain a dipole moment of 2.071 D [34] which is on the order of the dipole of water (1.85 D [47]). A range of indenocorannulenes have been synthesised [50] and electronic structure calculations suggested dipole moments from 3 to 4.5 D for PAH with eight to ten rings[15]. The nm-sized curved arenes known as nanocones, with curved nuclei that grow into large graphitic cones, have been fabricated with a clear number of pentagons integrated into the nucleus/tip of the nanocone [17, 28]. Electronic structure calculations of these nanocones showed a significant dipole for nanocones 0.5–4 nm in size ranging from ten to 35 D [29]. In another study, a nanotube cap (10,10) has been calculated to possess a dipole moment of 3.5 D [39].

Many applications are being explored for these molecules, centred around their dipole moment – for example, the flexoelectric response has been investigated for nanocones [29]. Large nanocones have been found to self-assemble into long filaments in an electric field, increasing the conductivity between the electrodes [26]. Some curved PAH, such as sumanene (Figure 1-**3a**), form crystal structures with 1D stacking [15] and have been suggested to possess a strong non-linear response for optical elements [33] and electronic transport properties for organic light emitting diodes [60]. The dipole moment is responsible for significant binding of curved PAH to metals which has been investigated as a method for electrical coupling between metals and organics in molecular electronics [4, 50] and also could improve ion capacity in lithium ion batteries [18].

The purpose of this paper is to calculate the dipole moment for a range of curved PAH molecules, determine the origin of the dipole moment and develop an atom-centered dis-

tributed multipole model of the electrostatic potential controlling the intermolecular interactions. This is an initial step towards the parametrisation of force fields needed for molecular dynamic simulations of systems containing curved PAHs, where the curvature-induced dipole produces the major long-range interaction and contributes significantly to the molecular interactions.

## 2 Computation of the charge distribution

A representative collection of known curved PAH were chosen to give a range of different geometries for analysis. Their curvature is due to pentagon integration and produces a dipole moment. We chose many structures in the size range of 10–20 rings, as these have been observed in non-graphitising carbon as determined from fringe analysis [7, 23, 68]. The set contains only molecules that fulfil the isolated pentagon rule formulated for fullerenes, according to which neighbouring pentagons are thermodynamically unstable and rearrange or expel $C_2$ to form pentagons isolated by hexagons [65]. Pericondensed PAH with high symmetry containing only $sp^2$ carbon atoms have been found to be stable due to $\pi$-delocalisation and are considered to be the primary species in high temperature amorphous carbons [49], and comprise the main part of the list in Figure 1 accordingly. Sumanene (**3a**) and (**3b**) contain $sp^3$ carbons and were also considered as they have been previously synthesised Sakurai [43], Wu et al. [63]. We shall refer to the terminating carbon atoms bonded to the hydrogen as to *rim carbon* atoms and to the central carbon atoms as to *hub* atoms.

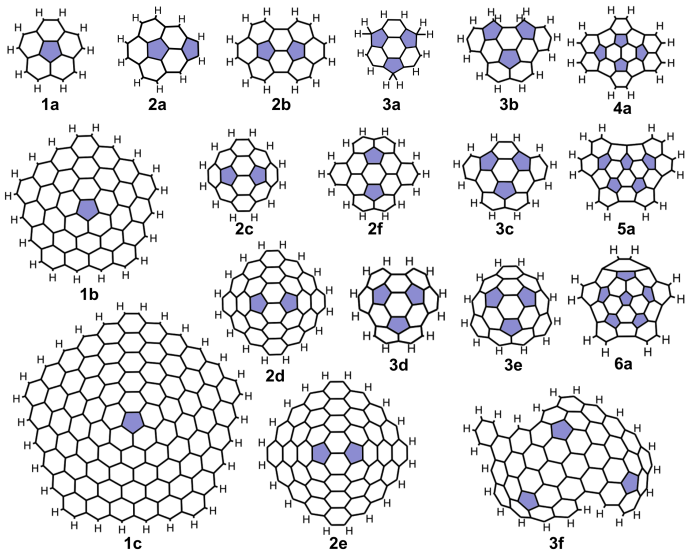


**Figure 1:** *The list of curved arenes considered in this work: corannulene **1a** [31], dicircumcorannulene **1b** and tricircumcorannulene **1c** [12], acecorannulene **2a** [1], [5,5]circulene **2b** [41], sumanene **3a** [43], acenaphth[3,2,1,8-fghij]-asindaceno-[3,2,1,8,7,6-pqrstuv]picene derivatives **3b**, **3c** and **2f** [11, 63], circumtrindene **3d** [46] and penta-benzocorannulene **6a** [44]. Pentagons are coloured for clarity.*

The calculation of the dipole moment of a molecule requires accurate molecular geometry and electron density. The hybrid density functional B3LYP [5, 32, 51] has been found to accurately describe both the geometry and the charge distribution of polyarenes and corannulene compared with experimentally determined values from synchrotron experiments [19, 40]. For a collection of 46 molecules it was found to predict the dipole to within 0.13 D of the experimental value (with the aug-cc-pVTZ basis set)[24]. Table 1 shows the dipole moment of corannulene as calculated with this functional compared to the post-Hartree-Fock method MP2 [38]. All geometries were optimised with a variety of basis sets, and calculated using the Gaussian 09 software [16]. The dipole moment of corannulene determined experimentally from the Stark effect is 2.071 D [34]. We find that for B3LYP the dipole moment converged to 2.044 D for the largest basis set (1400 functions) we used. As seen in Table 1, B3LYP yields a reasonably accurate dipole moment even with moderate sized basis sets where MP2 fails.

**Table 1:** *Dipole moment of corannulene calculated with B3LYP and MP2 methods, using basis sets with a different number of basis functions, in debye with % deviation from the experimental value of 2.071 D [34].*

| Basis set | Function no. | B3LYP | | MP2 | |
|---|---|---|---|---|---|
| 3-21G | 200 | 2.414 | (16.6%) | 2.777 | ( 34.1%) |
| 6-31G(d) | 320 | 1.722 | (16.9%) | 2.173 | (4.9%) |
| 6-311+G(d,p) | 500 | 2.187 | (5.6%) | 2.667 | (28.8%) |
| cc-pVTZ | 740 | 1.994 | (3.7%) | 2.419 | (16.8%) |
| cc-pVQZ | 1400 | 2.044 | (1.3%) | – | – |

In order to tackle the geometry optimisation of the larger structures we used the B3LYP/6-311+G(d,p) level of theory to optimise the geometry of the structures in Figure 1, with the exception of the largest structures, **1c** and **3f**, where geometry optimisation was performed using the smaller basis set 3-21G. The electronic structure was then calculated at the B3LYP/cc-pVQZ level of theory for all of the geometry optimised structures. This procedure (a B3LYP/6-311+G(d,p) geometry calculation used for the B3LYP/cc-pVQZ calculation of the electronic structure) led to a dipole moment for corannulene of 2.062 D, different by 0.45% from the experimental value. The coincidence is in part fortuitous, in view of the 1.3% deviation of the fully geometry-optimised corannulene structure at the cc-pVQZ level of theory from the experimental dipole, Table 1. The dipole moments can be found in Table 2.

# 3 Origin of the dipole moment

The dipole of curved arenes could originate from **(i)** a curvature-induced flexoelectric dipole from the polarisation of the $\pi$ bonds in direction normal to the C-skeleton [14, 25, 29]; **(ii)** the tilt angle of the C–H bonds [61]; **(iii)** charge transfer from the delocalised $\pi$-electrons in hexagonal sites to localised states on pentagonal sites [2, 9, 39, 59] or

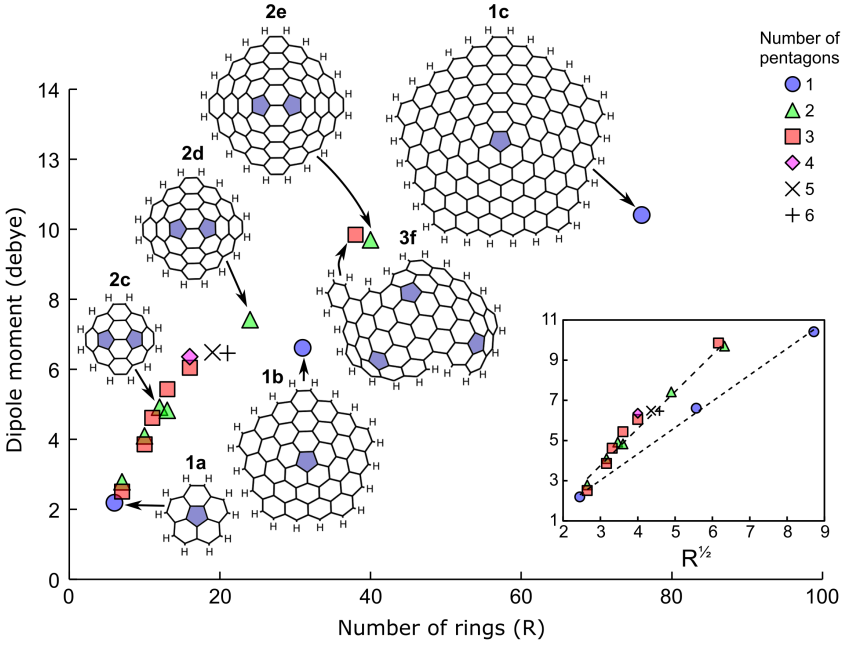


**Figure 2:** *Dipole moment of curved PAH molecules as a function of the number of rings. Inset: Dipole moment as a function of size comparing different numbers of pentagons.*

**(iv)** to localised states at the rim of the PAH [66]. To explore the importance of each of these factors, we first investigated the correlation of the dipole moment to the size of the molecule and the number of pentagons in it. Figure 2 shows the dipole moment as a function of the number of rings. The size dependency of the dipole for fragments of the C-skeleton of a nanocone has been found to be linear with the radius of the aromatic network [29]. We find a similar linear trend of the dipole as a function of the square root of the number of rings (which is proportional to the diameter of the fragment), i.e. the dipole moment of hydrogen-passivated curved PAH molecules also scales linearly with diameter (Figure 2, inset). The dipole moment increases with the number of pentagons in the PAH, but it soon saturates after two to three pentagonal rings have been incorporated, which was also found for nanocones [29]. Thus, for curved PAH with more than two pentagons, the dipole moment depends on the size but not on the number of pentagons.

To illustrate the effect of the curvature on the electrostatic potential through the effects (i-ii), flexoelectric effect and CH bonds, we compared in Figure 3 the potentials created by the flat PAH coronene with one of the curved PAH, corannulene (**1a**). In both cases, the excess positive charge is dominating the potential in the region of the hydrogen atoms and excess negative charge dominates above and below the plane of the aromatic system due to the $\pi$-electrons – this distribution provides the large quadrupole moment of these PAHs. A cross section along the z-y plane of the electrostatic potential $\phi$ demonstrates a significant difference between the flat and curved cases: a normal polarisation (relative to the aromatic plane) of the $\pi$-electron charge is apparent. The increased electron density on the convex face of the bowl leads to the large dipole moment of corannulene, as was

observed earlier [20]. An additional example is given in Figure S2 in A.1, where the $\pi$ electron localisation of artificially flattened and relaxed curved corannulene are compared. In the curved structure, the $\pi$ bonds at the hub of the molecule are visibly polarised in direction normal to the C skeleton of the corannulene – the increase of the $\pi$ electron density on the concave side of the molecular bowl leads to a Pauli expulsion of electron density to the convex side.

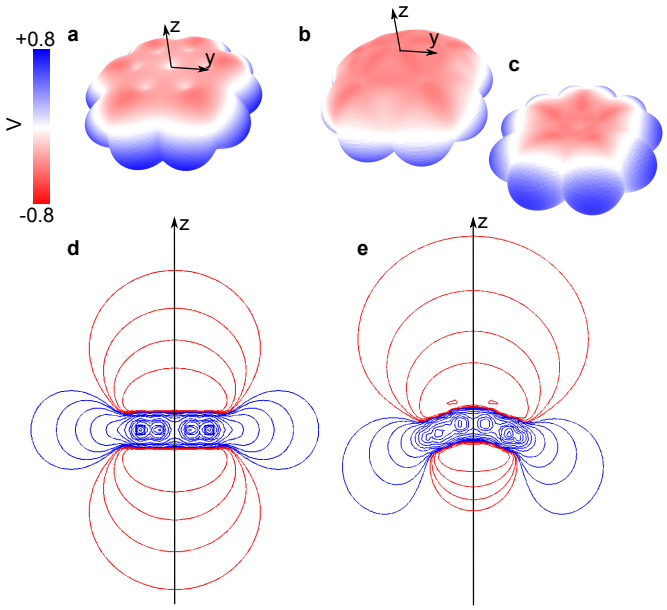


**Figure 3:** *Coronene and corannulene are shown left (a,d) and right (b,c,e). The molecular electrostatic potential was mapped to an isosurface of the electron density (B3LYP/cc-pVQZ, with an isovalue of 0.001 e Å$^{-3}$) (a,b,c). A two dimensional contour plot of the electrostatic potential through the z-y plane is shown (d,e), with the outermost four contour lines being drawn at ± 0.03, 0.06, 0.1 and 0.2 V.*

To illustrate the effects (iii) and (iv) from the localised states near the edge and at the pentagons, in Figure 4 we calculated for molecule **3f** the electron localisation function (ELF) – an analysis that has proved itself useful for curved PAHs [37]. The ELF is a measure of the likelihood of finding two electrons of the same spin in a small region of space. It is defined as [6]

$$\mathrm{ELF}(\mathbf{r}) = \left[1 + \frac{D(\mathbf{r})^2}{D_0(\mathbf{r})^2}\right]^{-1}, \tag{1}$$

where $D(\mathbf{r}) = \tau_\sigma(\mathbf{r}) - |\nabla\rho_\sigma(\mathbf{r})|^2/4\rho_\sigma(\mathbf{r})$ is proportional to the first non-vanishing coefficient in the Taylor expansion (with respect to small $|\mathbf{r}|$) of the spherically averaged conditional pair probability to find a same-spin electron in the vicinity of an electron in the vector-position $\mathbf{r}$; $\tau_\sigma = \sum_i^\sigma |\nabla\psi_i|^2$ is the kinetic energy density, $\rho_\sigma = \sum_i^\sigma \psi_i^*\psi_i$ is the $\sigma$-spin probability density, and $D_0(\mathbf{r}) = 9.12\rho_\sigma^{5/3}(\mathbf{r})$ is the value for a uniform electron gas. A value of ELF = 1 corresponds to a perfectly localised electron and ELF = 1/2 to a uniform electron gas. Figure 4 shows the iso-ELF surface (iso = 0.66), calculated using

the Multiwfn program [35], within which a region of localised electron pairing occurs. There appears greater localisation of the electrons (effect (iii)) at the pentagonal sites of **3f** compared to the hexagonal, cf. Figure 4 b. This is a known effect that has been studied in relation to the energetic barrier for inversion of the bowl [13], where the transition from flattened structure to curved decreases the aromatic delocalisation energy (cf. also A.1). There is also increased localisation in the rim region, effect (iv), Figure 4 c, in relation to the increased bond order of the C-C bonds at the rim [66].

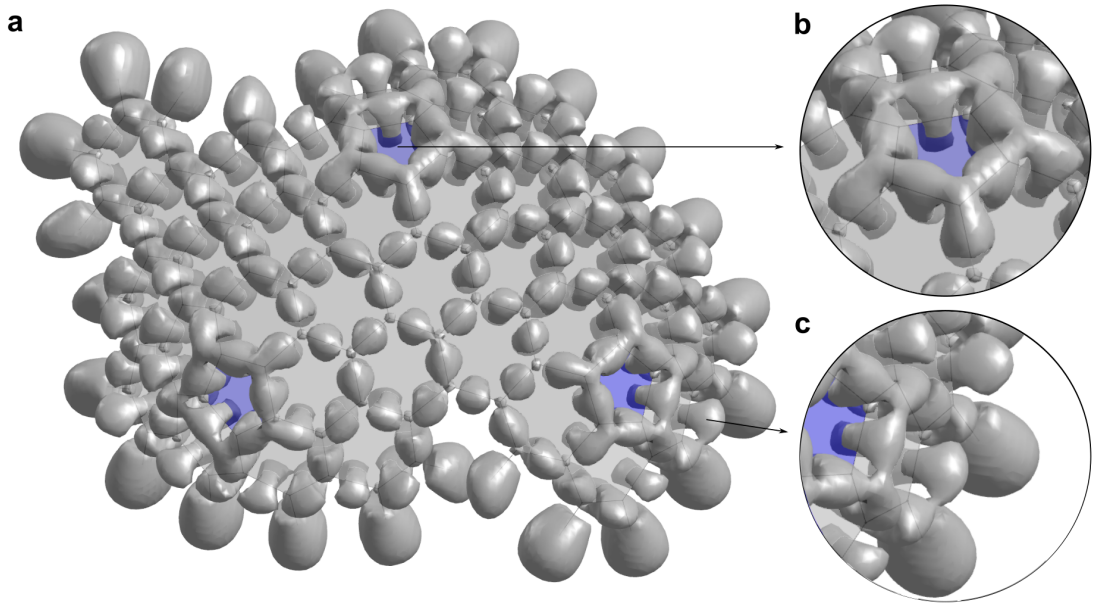


**Figure 4:** *a) Plot of the iso-surfaces of the electron localisation function for molecule **3f** at iso=0.66. Pentagonal rings are coloured blue and hexagonal rings grey to allow the molecular geometry to be seen. Insets show the localisation at pentagonal rings b) and localisation at the rim c).*

The local flexoelectric dipole $\boldsymbol{\mu}_{\text{flex}}$ (per C-site) due to curvature-induced $\pi$-bond polarisation in direction normal to the C-skeleton has been analysed using a tight binding rehybridisation model [14]; linear dependence with Haddon's pyramidalisation angle [21] has been demonstrated:

$$\boldsymbol{\mu}_{\text{flex}} = f_{\theta_{\text{p}}} \theta_{\text{p}} \mathbf{v}_{\pi}. \tag{2}$$

Here, $\mathbf{v}_{\pi}$ is the unit vector collinear with the axis of the $\pi$-orbital and pointing toward the concave side of the PAH, and $\theta_{\text{p}}$ the pyramidalisation angle, a characteristic of the deformation of the carbon skeleton (at each atom centre, a plane can be constructed that makes three equal angles $\theta_{\text{p}}$ with the adjacent C-C bonds; we refer to this plane as the *pyramidalisation plane*). The value of the flexoelectric constant $f_{\theta_{\text{p}}}$ of a $\pi$-orbital next to a $sp^2$ carbon atom between three hexagons has been calculated using electronic structure methods for fullerenes and nanotubes as $f_{\theta_{\text{p}}}$ = 2.34 D/rad [29]. Using the approach of these authors, we calculated a similar value of $f_{\theta_{\text{p}}}$= 2.35 D/rad for a (5,5) nanotube with the B3LYP/cc-pVQZ method we use. This flexoelectric coefficient is obviously unrelated to the localisation effects or the CH bond tilt.

The flexoelectric effect dominates the dipole moment of the curved PAHs we consider. This can be shown by neglecting the other three effects leading to polarisation. The summation of $\boldsymbol{\mu}_{\text{flex}}$, Eq 2, over all C-sites gives for the total dipole moment of the molecule

$$\boldsymbol{\mu} \approx \sum_{\text{C}_{\text{hub}}} \boldsymbol{\mu}_{\text{flex}} = f_{\theta_{\text{p}}} \boldsymbol{\theta}_{\text{tot}}, \tag{3}$$

where we refer to the vector $\boldsymbol{\theta}_{\text{tot}} = \sum_{\text{C}_{\text{hub}}} \theta_{\text{p}} \mathbf{v}_{\pi}$ as to the *total pyramidalisation* of the molecule. The rim C-atoms (bonded to hydrogen) are neglected in this sum, with the assumption that the Pauli expulsion is much less effective for the two adjacent $\pi$ orbitals next to a rim C compared to three $\pi$ orbitals next to a hub C. We also excluded the $sp^3$ carbon atoms (having no $\pi$-orbitals) in **3a** and **3b**. To determine the vector $\mathbf{v}_{\pi}$, we used the POAV2 approach of Haddon [21], in which six conditions for orthogonality of the hybridised orbitals of the form $1 + \lambda_i \lambda_j \mathbf{v}_i \cdot \mathbf{v}_j = 0$, where $i, j = 1, 2, 3, \pi$, are used determine the four hybridisations $\lambda_i$ and to express $\mathbf{v}_{\pi}$ as a linear combination of the unit vectors $\mathbf{v}_{1,2,3}$ defined by the C-C bonds. Note that this $\mathbf{v}_{\pi}$ can be quite different from the normal vector to the pyramidalisation plane (which is used often as an approximation of $\mathbf{v}_{\pi}$ within the POAV1 approach [21]). If the contributions to $\mu$ of the localisation effects and the CH bond tilt are small, the dipole moment of all molecules we investigate must be proportional to $\boldsymbol{\theta}_{\text{tot}}$, with proportionality coefficient $f_{\theta_{\text{p}}}$. This is indeed the case, as demonstrated in Figure 5; the linear relationship 3 holds with $R^2$ = 0.995 and the value of the linear coefficient is $f_{\theta_{\text{p}}} = 2.24 \pm 0.03$ D/rad (all errors are $2\sigma$). This value differs by 4.7% from the one calculated for a nanotube, i.e. more than 95% of the dipole of the curved PAHs is of flexoelectric origin. The contribution of the other three effects is surprisingly small, in part due to a compensation of effects (discussed in A.1). We attempted to elaborate on the geometrical model 3 by including the contribution of the C–H bond dipole and considering different values of $f_{\theta_{\text{p}}}$ for carbon in pentagons and at the rim, but this did not significantly improve the agreement with the computed dipoles. Eq 3 allows the calculation of the dipole moment of a curved arene from our list with an average error of 2.3±1.9%, which is a satisfactory accuracy in view of the expected error of the DFT values (cf. Table 2).

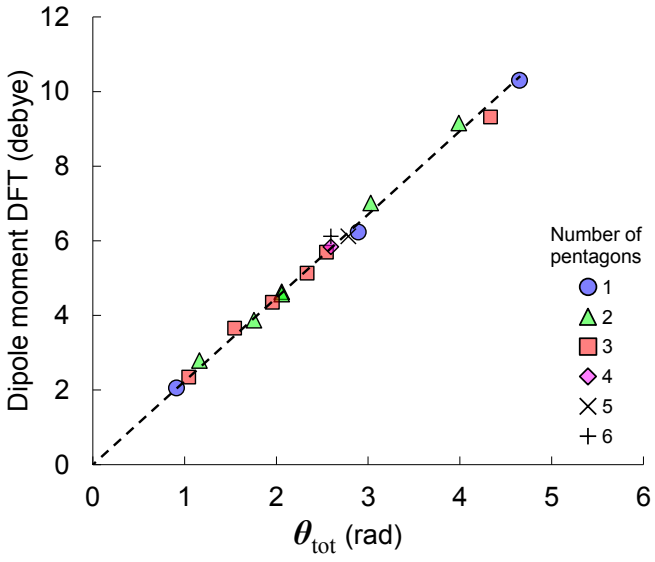


**Figure 5:** *Values of $\theta_{tot}$ Eq 3 compared with the calculated DFT dipole moment for the set of molecules in Figure 1, cf. Table 2. The number of pentagons for each fragment is also indicated.*

# 4 Distributed multipole description

Curved aromatic structures play a role in numerous technologically relevant processes, and the interest towards modelling the interactions within these materials is growing. One such process of interest to us is the role of the curved PAHs' dipole in soot formation. A strong correlation is known to exist between soot formation and chemi-ions in a flame [8], but Chen and Wang recently calculated binding energies between flat PAH and flame chemi-ions that are not strong enough to stabilise anything larger than a dimer [10]. One can expect the situation to be qualitatively different with curved PAH due to strong long-range ion-dipole interaction, which might be involved in stabilising clusters of PAHs, but an appropriate force field is required to study this case. A second example is the adsorption in microporous carbon. The effect of the curvature has been explored, e.g., for hydrogen absorption, which is enhanced on corannulene due to a dipole-induced dipole interaction [45] modelled with molecular dynamics via modification of the van der Waals parameters of the force field. Obviously, in cases of adsorption of polar molecules on microporous carbon, a strong directional solid dipole-solid dipole interaction will control the process – in this case, an effective van der Waals model of the flexoelectric dipole is inapplicable. The strained pentagon presents a binding site for ions as well [58] (which is probably the reason why corannulene allows for supercharging of lithium in battery applications [70]), and force fields are also required for this case. The most common representation of the charge distribution in a molecule used in force fields is an ensemble of atom-centred point charges. However, this model is unsuitable for curved PAHs, where the most long-ranged interaction is due to the flexoelectric dipole that cannot be represented with atom-centred point charges. Therefore, we will now investigate the capability of a distributed multipole [52] description of the electrostatic potential of curved PAHs.

**Table 2:** *Dipole moment and pyramidalisation of the curved aromatic hydrocarbons in Figure 1: DFT dipole values (B3LYP method) compared with the model Eq 3, and total and maximum pyramidalisation angles.*

| Molecule | DFT dipole $\mu$ [D] | max. pyr. angle $\max(\theta_p)$ [°] | total pyr. $\theta_{tot} = \sum_{C_{hub}} \theta_p \mathbf{v}_\pi$ [rad] | flexoel. dipole $\sum_{C_{hub}} \boldsymbol{\mu}_{flex}$ [D] |
|---|---|---|---|---|
| 1a | 2.06 | 8.34 | 0.909 | 2.03 |
| 1b | 6.24 | 10.48 | 2.89 | 6.46 |
| 1c | 10.30 | 10.59 | 4.65 | 10.39 |
| 2a | 2.79 | 10.99 | 1.16 | 2.59 |
| 2b | 3.87 | 11.23 | 1.75 | 3.92 |
| 2c | 4.63 | 11.63 | 2.06 | 4.60 |
| 2d | 7.01 | 11.91 | 3.03 | 6.76 |
| 2e | 9.15 | 11.59 | 3.99 | 8.92 |
| 2f | 4.57 | 10.65 | 2.06 | 4.60 |
| 3a | 2.34 | 8.85 | 1.04 | 2.33 |
| 3b | 3.66 | 12.51 | 1.54 | 3.45 |
| 3c | 4.35 | 12.35 | 1.96 | 4.37 |
| 3d | 5.13 | 12.08 | 2.33 | 5.21 |
| 3e | 5.70 | 12.17 | 2.54 | 5.69 |
| 3f | 9.32 | 10.64 | 4.33 | 9.69 |
| 4a | 5.84 | 12.52 | 2.59 | 5.80 |
| 5a | 6.12 | 12.28 | 2.78 | 6.22 |
| 6a | 6.12 | 12.09 | 2.59 | 5.80 |

The expansion of the electrostatic potential in an ensemble of multipole centres (a set of atom-centred charge, dipole, quadrupole, etc.) is not unique – different sets of values of the multipoles at each centre can produce the same total potential; therefore, no physical meaning should be ascribed to the values of the multipoles in a distributed multipole expansion. Nevertheless, we sought a decomposition that not only describes the electrostatic potential outside the van der Waals surface correctly, but is also physically reasonable. We tested two methods which are commonly employed for the decomposition: the Gaussian distributed multipole analysis (GDMA) [52] and the atoms in molecules (AIM) approach [3]. The advantage of the AIM approach is that the electron density itself is partitioned and then integrated to yield the multipoles in the atomic basins, making the decomposition independent of the basis set of molecular orbitals used and the system size [36]. On the other hand, GDMA computes the multipoles directly from the Gaussian basis functions and is fast even for the largest structures we studied, and is more widely used (GDMA point multipoles have been integrated into molecular dynamics packages such as AMOEBA, CHARMM and DL_MULTI). Two variants of GDMA were employed: one with rank 2 multipoles (point charge-dipole-quadrupole) on every atom, to which we refer as to GDMA($C_2H_2$), and another with rank 2 multipoles on every carbon but only a point charge (rank 0 restriction) on every hydrogen, GDMA($C_2H_0$). For the PAHs in Figure 1, both methods produce total dipole moment of magnitude within $\pm 0.001$ D of the exact $\mu$

that follows from the electronic structure calculations. For the smaller structures we found an agreement between the AIM and GDMA($C_2H_2$) atom-centred dipole vectors; however, the larger structures had significant divergence – this is demonstrated in A.2. On the other hand, GDMA($C_2H_0$) and AIM agree reasonably in all cases.

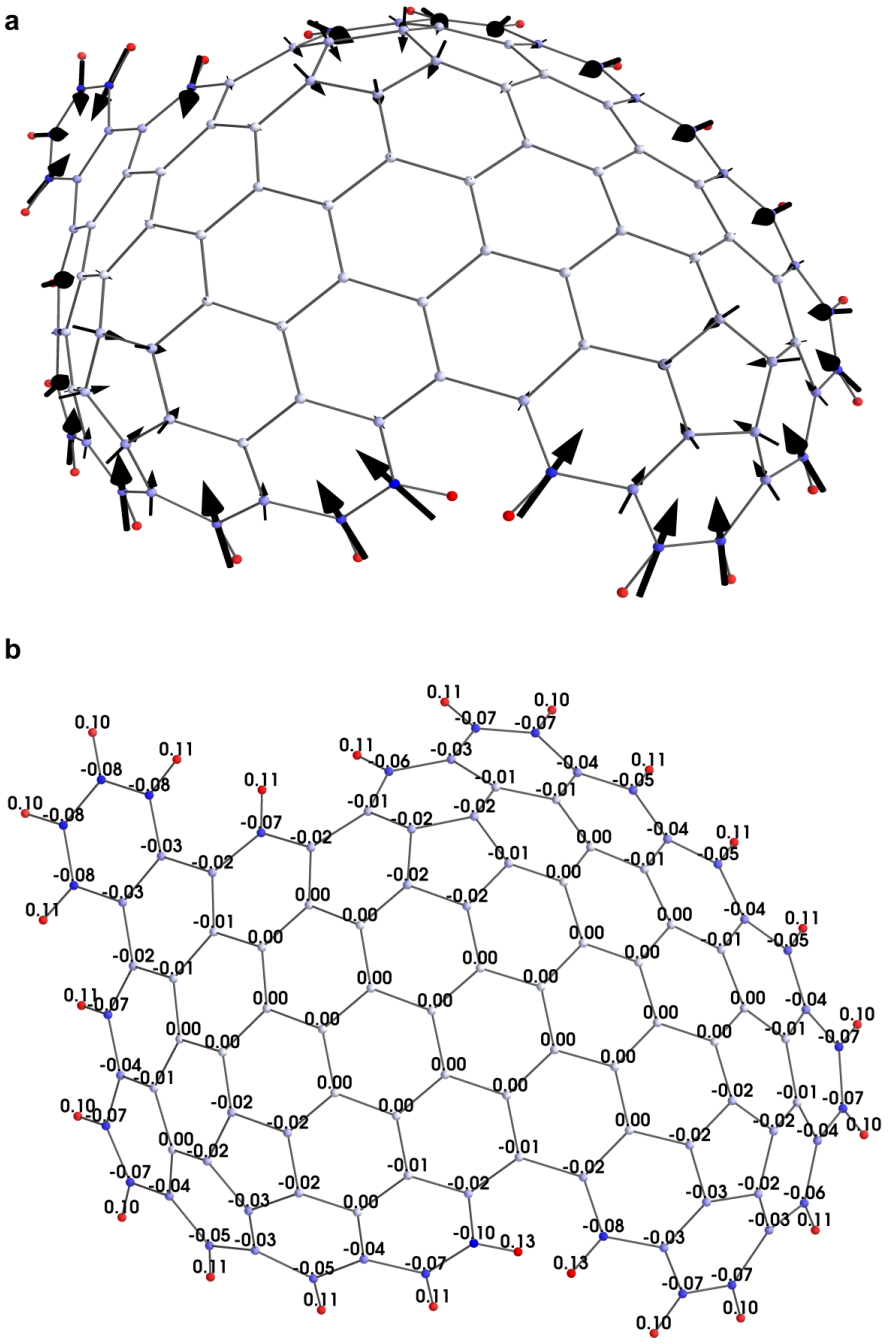


**Figure 6:** *GDMA dipoles a) and partial charges b) for the molecule **3f** with the dipoles shown as vectors and partial charge values printed at the atomic sites.*

Figure 6 shows the GDMA($C_2H_0$) distributed point dipoles and monopoles for molecule

**3f**. The C-centred dipole moments range between 0.11-0.79 D in magnitude. The procedure computes a large dipole at each rim carbon atom, in the direction of the C-H bond with the positive pole pointing toward the hub. This polarisation reflects mostly the localised states at the rim of the PAH (increased bond orders and electron density near the rim compared to the hub [66], effect (iv)). In the GDMA($C_2H_0$) decomposition, the polarisation of the C-H bonds (and effect (ii)) is reflected by the partial charges at the C and H atoms. From the dipole at each pyramidalised hub C-atom and the local $\theta_p$, we obtain "local values" for the flexoelectric coefficient $f_{\theta_p}$ in the range 2.24–2.27 D/rad, which coincide with the "averaged" $f_{\theta_p}$ value in Eq 3 and Figure 5. The largest contributors to the net dipole moment are the pentagonal carbon atoms that are the most heavily pyramidalised. The total dipole moment per pentagonal ring (defined as the vector sum of the GDMA($C_2H_0$) dipoles of all atoms in the pentagon) was found to be of magnitude 1.76±0.03 D. Finally, in Figure 6 c, the partial charges at the pentagonal carbon atoms are found to range between -0.01 and -0.03 *e*, and each pentagon contains a total charge of -0.09±0.02 *e* (effect (iii)). This value is slightly less than what has previously been predicted for the pentagonal charge accumulation in nanotube end caps, -0.013 *e* (calculated using the PBE density functional, with plane wave basis functions up of 25 and 225 Ry for the valance and charge density, respectively) [39, 59]. Thus, all four polarisation effects are well represented by the GDMA($C_2H_0$) distributed multipole expansion.

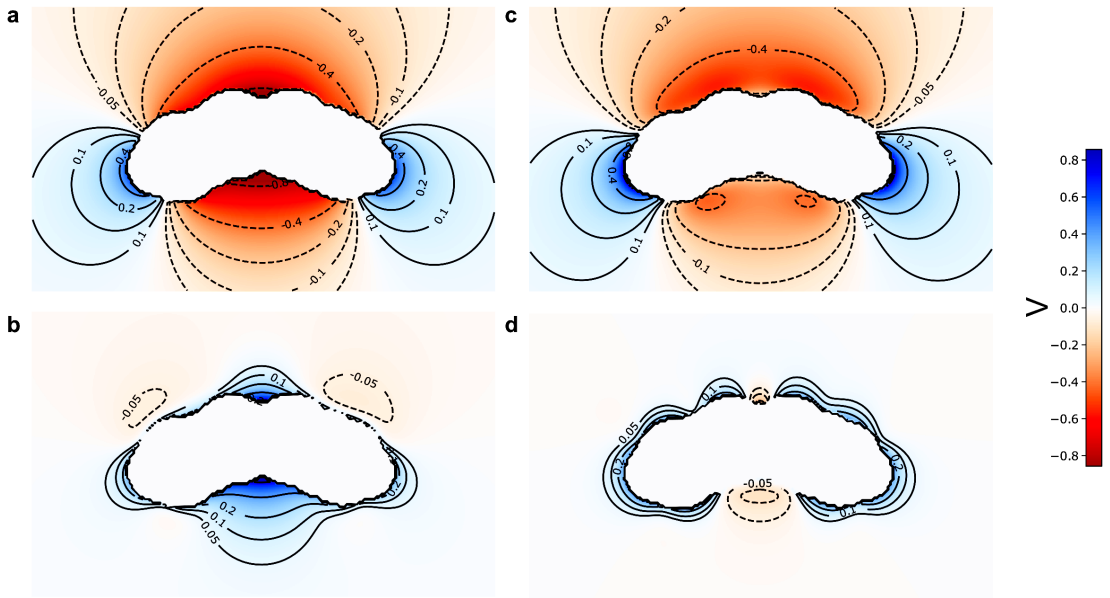


**Figure 7:** *Electrostatic potential along the $z-y$ plane for corannulene (**1a**) calculated from a) the point charge model obtained by the MK scheme, and c) the GDMA($C_2H_0$) multipole representation. Potential maps of the difference between these potentials and the DFT result in Figure 3e are given in b-d) for the point charge b) and in d) for the multipole model.*

Figure 7 shows the electrostatic potential on the $z-y$ plane outside the van der Waals surface of corannulene for two different multipole decompositions: 7c is GDMA($C_2H_0$) and 7a is the standard point charge description as obtained by the Merz-Kollman (MK)

scheme. In 7b and d, the difference between these potentials and the exact DFT potential in Figure 3 is given (we used the procedure of Kramer et al. [27]). A significant divergence between the point charge ensemble's potential and the DFT potential is evident, especially near the pentagonal carbon atoms where the flexoelectric dipole is large; on the other hand, the GDMA($C_2H_0$) representation is accurate. In order to quantify the differences, the molecular electrostatic potential was calculated at the electron density isosurface 0.002 $e/\text{Å}^3$ (near the interaction surface of molecular pairs). For the point charge model, the average difference between the DFT and the model potentials at this surface was 36%. This error was reduced to 2.6% for the GDMA($C_2H_0$) distributed multipole representation. An additional problem of the MK description is that the total dipole moment of the point charge ensemble is 1.73 D, a value reduced by 21% compared with the DFT dipole. GDMA($C_2H_0$) also produced reasonable total quadrupole moments (within 12% of the DFT results) which is not the case with the point charge model.

# 5 Conclusion

The dipole moment $\mu$ of 18 curved aromatic molecules has been computed and was shown to reach significant values (2-10 D). The main contribution to this moment was shown to stem from the $\pi$-orbital flexoelectric dipole moment: $\mu$ of all these molecules can be calculated with 95% accuracy using a standard linear model for the dependence of the flexoelectric polarisation on the pyramidalisation at each carbon atom. Gaussian distributed multipole expansion, restricted to rank 2 at the carbon atoms and rank 0 at the hydrogens – GDMA($C_2H_0$) – has been shown to reproduce the electrostatic potential of the curved arenes with sufficient accuracy. We have previously applied distributed multipole analysis to describe the potential of flat PAH molecules and found it improved on point charge models, allowing the reproduction of the second virial coefficient of benzene [57]. Yet, for dimers of flat PAH molecules, a point charge distribution is sufficient for developing an accurate force field (iso-PAHAP) [56, 57]. Here we show that for curved PAHs, this is not the case. The common atom-centred point charge models fail to correctly reproduce the $\pi$-electron flexoelectric dipole moment, which controls the long range potential and contributes significantly to the short range interactions. Therefore, atom-centred point charge ensembles are inapplicable as a basis for force fields for molecular dynamic simulations of curved PAHs.

# Acknowledgements

This project is supported by the National Research Foundation (NRF), Prime Minister's Office, Singapore under its Campus for Research Excellence and Technological Enterprise (CREATE) programme. We would also like to thank Dr Grant McIntosh, University of Auckland, for his aid in performing the strained corannulene calculations.

# References


[1] A. H. Abdourazak, A. Sygula, and P. W. Rabideau. "Locking" the bowl-shaped geometry of corannulene: cyclopentacorannulene. *Journal of the American Chemical Society*, 115(7):3010–3011, 1993. doi:10.1021/ja00060a073.

[2] B. An, S. Fukuyama, K. Yokogawa, M. Yoshimura, M. Egashira, Y. Korai, and I. Mochida. Single pentagon in a hexagonal carbon lattice revealed by scanning tunneling microscopy. *Applied Physics Letters*, 78(23):3696–3698, 2001.

[3] R. F. Bader. *Atoms in molecules*. Clarendon Press, 1994.

[4] T. Bauert, L. Zoppi, G. Koller, A. Garcia, K. K. Baldridge, and K. H. Ernst. Large induced interface dipole moments without charge transfer: Buckybowls on metal surfaces. *Journal of Physical Chemistry Letters*, 2(21):2805–2809, 2011. doi:10.1021/jz2012484.

[5] A. D. Becke. Density-functional thermochemistry. III. The role of exact exchange. *The Journal of Chemical Physics*, 98(7):5648, 1993. doi:10.1063/1.464913.

[6] A. D. Becke and K. E. Edgecombe. A simple measure of electron localization in atomic and molecular systems. *The Journal of Chemical Physics*, 92(9):5397–5403, 1990. doi:10.1063/1.458517.

[7] M. L. Botero, E. M. Adkins, S. González-Calera, H. Miller, and M. Kraft. PAH structure analysis of soot in a non-premixed flame using high-resolution transmission electron microscopy and optical band gap analysis. *Combustion and Flame*, 164:250–258, 2016. doi:10.1016/j.combustflame.2015.11.022.

[8] H. F. Calcote, D. B. Olson, and D. G. Keil. Are ions important in soot formation? *Energy & Fuels*, 2(4):494–504, 1988. doi:10.1021/ef00010a016.

[9] D. Carroll, P. Redlich, P. Ajayan, J. Charlier, X. Blase, A. De Vita, and R. Car. Electronic Structure and Localized States at Carbon Nanotube Tips. *Physical Review Letters*, 78(14):2811–2814, 1997. doi:10.1103/PhysRevLett.78.2811.

[10] D. Chen and H. Wang. Cation-$\pi$ Interactions between Flame Chemiions and Aromatic Compounds. *Energy & Fuels*, 31(3):2345–2352, 2017. doi:10.1021/acs.energyfuels.6b02354.

[11] D. Chen, T. S. Totton, J. W. J. Akroyd, S. Mosbach, and M. Kraft. Size-dependent melting of polycyclic aromatic hydrocarbon nano-clusters: A molecular dynamics study. *Carbon*, 67:79–91, 2014. doi:10.1016/j.carbon.2013.09.058.

[12] J. R. Dias. Resonance Topology of Fluoranthenoid/Fluorenoid Hydrocarbons and Related Systems. *Polycyclic Aromatic Compounds*, 31(1):48–60, 2011. doi:10.1080/10406638.2011.545732.

[13] M. A. Dobrowolski, A. Ciesielski, and M. K. Cyrański. On the aromatic stabilization of corannulene and coronene. *Physical Chemistry Chemical Physics*, 13(46):20557, 2011. doi:10.1039/c1cp21994d.

[14] T. Dumitrică, C. M. Landis, and B. I. Yakobson. Curvature-induced polarization in carbon nanoshells. *Chemical Physics Letters*, 360(1-2):182–188, 2002. doi:10.1016/S0009-2614(02)00820-5.

[15] A. S. Filatov, L. T. Scott, and M. A. Petrukhina. $\pi$-$\pi$ Interactions and Solid State Packing Trends of Polycyclic Aromatic Bowls in the Indenocorannulene Family: Predicting Potentially Useful Bulk Properties. *Crystal Growth & Design*, 10(10): 4607–4621, 2010. doi:10.1021/cg100898g.

[16] M. J. Frisch, G. W. Trucks, H. B. Schlegel, G. E. Scuseria, M. A. Robb, J. R. Cheeseman, G. Scalmani, V. Barone, G. A. Petersson, H. Nakatsuji, X. Li, M. Caricato, A. Marenich, J. Bloino, B. G. Janesko, R. Gomperts, B. Mennucci, H. P. Hratchian, J. V. Ortiz, A. F. Izmaylov, J. L. Sonnenberg, D. Williams-Young, F. Ding, F. Lipparini, F. Egidi, J. Goings, B. Peng, A. Petrone, T. Henderson, D. Ranasinghe, V. G. Zakrzewski, J. Gao, N. Rega, G. Zheng, W. Liang, M. Hada, M. Ehara, K. Toyota, R. Fukuda, J. Hasegawa, M. Ishida, T. Nakajima, Y. Honda, O. Kitao, H. Nakai, T. Vreven, K. Throssell, J. A. Montgomery, J. E. Peralta, F. Ogliaro, M. Bearpark, J. J. Heyd, E. Brothers, K. N. Kudin, V. N. Staroverov, T. Keith, R. Kobayashi, J. Normand, K. Raghavachari, A. Rendell, J. C. Burant, S. S. Iyengar, J. Tomasi, M. Cossi, J. M. Millam, M. Klene, C. Adamo, R. Cammi, J. W. Ochterski, R. L. Martin, K. Morokuma, O. Farkas, J. B. Foresman, and D. J. Fox. Gaussian 09, Revision A 02.

[17] M. Ge and K. Sattler. Observation of fullerene cones. *Chemical Physics Letters*, 220 (3-5):192–196, 1994. doi:10.1016/0009-2614(94)00167-7.

[18] R. Gerald, C. Johnson, J. Rathke, R. Klingler, G. Sandí, and L. Scanlon. $^{7}$Li NMR study of intercalated lithium in curved carbon lattices. *Journal of Power Sources*, 89 (2):237–243, 2000. doi:10.1016/S0378-7753(00)00435-3.

[19] S. Grabowsky, M. Weber, Y. S. Chen, D. Lentz, B. M. Schmidt, M. Hesse, and P. Luger. Electron density of corannulene from synchrotron data at 12 K, comparison with fullerenes. *Zeitschrift fur Naturforschung - Section B Journal of Chemical Sciences*, 65(4):452–460, 2010. doi:10.1515/znb-2010-0403.

[20] S. Grimme, J. Antony, T. Schwabe, and C. Mück-Lichtenfeld. Density functional theory with dispersion corrections for supramolecular structures, aggregates, and complexes of (bio)organic molecules. *Organic & Biomolecular Chemistry*, 5(5): 741–758, 2007. doi:10.1039/b615319b.

[21] R. C. Haddon. Hybridization and the orientation and alignment of $\pi$-orbitals in nonplanar conjugated organic molecules: $\pi$-orbital axis vector analysis (POAV2). *Journal of the American Chemical Society*, 108(11):2837–2842, 1986. doi:10.1021/ja00271a009.

[22] P. J. F. Harris. Fullerene-related structure of commercial glassy carbons. *Philosophical Magazine*, 84(29):3159–3167, 2004. doi:10.1080/14786430410001720363.

[23] P. J. F. Harris, Z. Liu, and K. Suenaga. Imaging the atomic structure of activated carbon. *Journal of Physics: Condensed Matter*, (36):362201. doi:10.1088/0953-8984/20/36/362201.

[24] A. L. Hickey and C. N. Rowley. Benchmarking quantum chemical methods for the calculation of molecular dipole moments and polarizabilities. *The Journal of Physical Chemistry A*, 118(20):3678–3687, 2014. doi:10.1021/jp502475e.

[25] S. V. Kalinin and V. Meunier. Electronic flexoelectricity in low-dimensional systems. *Physical Review B*, 77(3):1–4, 2008. doi:10.1103/PhysRevB.77.033403.

[26] M. Knaapila, O. T. Rømoen, E. Svåsand, J. P. Pinheiro, Ø. G. Martinsen, M. Buchanan, A. T. Skjeltorp, and G. Helgesen. Conductivity Enhancement in Carbon Nanocone Adhesive by Electric Field Induced Formation of Aligned Assemblies. *ACS Applied Materials & Interfaces*, 3(2):378–384, 2011. doi:10.1021/am100990c.

[27] C. Kramer, P. Gedeck, and M. Meuwly. Atomic multipoles: Electrostatic potential fit, local reference axis systems, and conformational dependence. *Journal of Computational Chemistry*, 33(20):1673–1688, 2012. doi:10.1002/jcc.22996.

[28] A. Krishnan, E. Dujardin, M. M. J. Treacy, J. Hugdahl, S. Lynum, and T. W. Ebbesen. Graphitic cones and the nucleation of curved carbon surfaces. *Nature*, 388 (6641):451–454, 1997. doi:10.1038/41284.

[29] A. G. Kvashnin, P. B. Sorokin, and B. I. Yakobson. Flexoelectricity in Carbon Nanostructures: Nanotubes, Fullerenes, and Nanocones. *The Journal of Physical Chemistry Letters*, 6(14):2740–2744, 2015. doi:10.1021/acs.jpclett.5b01041.

[30] A. L. Lafleur, J. B. Howard, J. A. Marr, and T. Yadav. Proposed fullerene precursor corannulene identified in flames both in the presence and absence of fullerene production. *The Journal of Physical Chemistry*, 97(51):13539–13543, 1993. doi:10.1021/j100153a020.

[31] R. G. Lawton and W. E. Barth. Synthesis of corannulene. *Journal of the American Chemical Society*, 93(7):1730–1745, 1971. doi:10.1021/ja00736a028.

[32] C. Lee, W. Yang, and R. G. Parr. Development of the Colle-Salvetti correlation-energy formula into a functional of the electron density. *Physical Review B*, 37(2): 785–789, 1988. doi:10.1103/PhysRevB.37.785.

[33] W. Li, X. Zhou, W. Q. Tian, and X. Sun. A new scheme for significant enhancement of the second order nonlinear optical response from molecules to ordered aggregates. *Physical Chemistry Chemical Physics*, 15(6):1810, 2013. doi:10.1039/c2cp43536e.

[34] F. J. Lovas, R. J. McMahon, J. U. Grabow, M. Schnell, J. Mack, L. T. Scott, and R. L. Kuczkowski. Interstellar chemistry: A strategy for detecting polycyclic aromatic hydrocarbons in space. *Journal of the American Chemical Society*, 127(12):4345–4349, 2005. doi:10.1021/ja0426239.

[35] T. Lu and F. Chen. Multiwfn: a multifunctional wavefunction analyzer. *Journal of Computational Chemistry*, 33(5):580–592, 2012.

[36] C. F. Matta and R. J. Boyd, editors. *The Quantum Theory of Atoms in Molecules*. Wiley-VCH Verlag GmbH & Co. KGaA, Weinheim, Germany, 2007. doi:10.1002/9783527610709.

[37] S. Mebs, M. Weber, P. Luger, B. M. Schmidt, H. Sakurai, S. Higashibayashi, S. Onogi, and D. Lentz. Experimental electron density of sumanene, a bowl-shaped fullerene fragment; comparison with the related corannulene hydrocarbon. *Organic & Biomolecular Chemistry*, 10(11):2218, 2012.

[38] C. Möller and M. S. Plesset. Note on an Approximation Treatment for Many-Electron Systems. *Physical Review*, 46(7):618–622, 1934. doi:10.1103/PhysRev.46.618.

[39] M. Otani, S. Okada, and Y. Okamoto. Intrinsic dipole moment on the capped carbon nanotubes. *Physical Review B - Condensed Matter and Materials Physics*, 80(15): 4–6, 2009. doi:10.1103/PhysRevB.80.153413.

[40] M. A. Petrukhina, K. W. Andreini, J. Mack, and L. T. Scott. X-ray quality geometries of geodesic polyarenes from theoretical calculations: What levels of theory are reliable? *Journal of Organic Chemistry*, 70(14):5713–5716, 2005. doi:10.1021/jo050233e.

[41] P. W. Rabideau, A. H. Abdourazak, H. E. Folsom, Z. Marcinow, A. Sygula, and R. Sygula. Buckybowls: Synthesis and ab Initio Calculated Structure of the First Semibuckminsterfullerene. *Journal of the American Chemical Society*, 116(17): 7891–7892, 1994. doi:10.1021/ja00096a054.

[42] H. Richter, A. J. Labrocca, W. J. Grieco, K. Taghizadeh, A. L. Lafleur, and J. B. Howard. Generation of Higher Fullerenes in Flames. *Journal of Physical Chemistry B*, 101(9):1556–1560, 1997. doi:10.1021/jp962928c.

[43] H. Sakurai. A Synthesis of Sumanene, a Fullerene Fragment. *Science*, 301(5641): 1878–1878, 2003. doi:10.1126/science.1088290.

[44] G. N. Sastry, E. D. Jemmis, G. Mehta, and S. R. Shah. Synthetic strategies towards $C_{60}$. Molecular mechanics and MNDO study on sumanene and related structures. *Journal of the Chemical Society, Perkin Transactions 2*, (10):1867, 1993. doi:10.1039/p29930001867.

[45] L. G. Scanlon, P. B. Balbuena, Y. Zhang, G. Sandi, C. K. Back, W. A. Feld, J. Mack, M. A. Rottmayer, and J. L. Riepenhoff. Investigation of corannulene for molecular hydrogen storage via computational chemistry and experimentation. *Journal of Physical Chemistry B*, 110(15):7688–7694, 2006. doi:10.1021/jp0574403.

[46] L. T. Scott, M. S. Bratcher, and S. Hagen. Synthesis and Characterization of a $C_{36}H_{12}$ Fullerene Subunit. *Journal of the American Chemical Society*, 118(36):8743–8744, 1996. doi:10.1021/ja9621511.

[47] S. L. Shostak, W. L. Ebenstein, and J. S. Muenter. The dipole moment of water. I. Dipole moments and hyperfine properties of $H_2O$ and HDO in the ground and excited vibrational states. *The Journal of Chemical Physics*, 94(9):5875, 1991. doi:10.1063/1.460471.

[48] R. Singh and M. Frenklach. A mechanistic study of the influence of graphene curvature on the rate of high-temperature oxidation by molecular oxygen. *Carbon*, 101: 203–212, 2016. doi:10.1016/j.carbon.2016.01.090.

[49] S. E. Stein and A. Fahr. High-temperature stabilities of hydrocarbons. *The Journal of Physical Chemistry*, 89(17):3714–3725, 1985. doi:10.1021/j100263a027.

[50] B. D. Steinberg, E. A. Jackson, A. S. Filatov, A. Wakamiya, M. A. Petrukhina, and L. T. Scott. Aromatic $\pi$-Systems More Curved Than $C_{60}$. The Complete Family of All Indenocorannulenes Synthesized by Iterative Microwave-Assisted Intramolecular Arylations. *Journal of the American Chemical Society*, 131(30):10537–10545, 2009. doi:10.1021/ja9031852.

[51] P. J. Stephens, F. J. Devlin, C. F. Chabalowski, and M. J. Frisch. Ab Initio Calculation of Vibrational Absorption and Circular Dichroism Spectra Using Density Functional Force Fields. *The Journal of Physical Chemistry*, 98(45):11623–11627, 1994. doi:10.1021/j100096a001.

[52] A. Stone. *The Theory of Intermolecular Forces*. Oxford University Press, 2013. doi:10.1093/acprof:oso/9780199672394.001.0001.

[53] D. S. Su, R. E. Jentoft, J. O. Müller, D. Rothe, E. Jacob, C. D. Simpson, Ž. Tomović, K. Müllen, A. Messerer, U. Pöschl, R. Niessner, and R. Schlögl. Microstructure and oxidation behaviour of Euro IV diesel engine soot: a comparative study with synthetic model soot substances. *Catalysis Today*, 90(1-2):127–132, 2004. doi:10.1016/j.cattod.2004.04.017.

[54] A. P. Terzyk, S. Furmaniak, P. J. F. Harris, P. A. Gauden, J. Włoch, P. Kowalczyk, and G. Rychlicki. How realistic is the pore size distribution calculated from adsorption isotherms if activated carbon is composed of fullerene-like fragments? *Physical Chemistry Chemical Physics*, 9(44):5919, 2007. doi:10.1039/b710552e.

[55] A. P. Terzyk, S. Furmaniak, P. A. Gauden, P. J. Harris, and P. Kowalczyk. Virtual Porous Carbons. In *Novel Carbon Adsorbents*, pages 61–104. Elsevier, 2012. doi:10.1016/B978-0-08-097744-7.00003-X.

[56] T. S. Totton, A. J. Misquitta, and M. Kraft. A First Principles Development of a General Anisotropic Potential for Polycyclic Aromatic Hydrocarbons. *Journal of Chemical Theory and Computation*, 6(3):683–695, 2010. doi:10.1021/ct9004883.

[57] T. S. Totton, A. J. Misquitta, and M. Kraft. Assessing the Polycyclic Aromatic Hydrocarbon Anisotropic Potential with Application to the Exfoliation Energy of Graphite. *The Journal of Physical Chemistry A*, 115(46):13684–13693, 2011. doi:10.1021/jp208088s.

[58] D. Vijay, H. Sakurai, V. Subramanian, and G. N. Sastry. Where to bind in buckybowls? The dilemma of a metal ion. *Physical Chemistry Chemical Physics*, 14(9): 3057, 2012. doi:10.1039/c2cp22087c.

[59] A. D. Vita, J. Charlier, X. Blase, and R. Car. Electronic structure at carbon nanotube tips. *Applied Physics A*, 68(3):283–286, 1999. doi:10.1007/s003390050889.

[60] B. T. Wang, M. A. Petrukhina, and E. R. Margine. Electronic transport properties of selected carbon $\pi$-bowls with different size, curvature and solid state packing. *Carbon*, 94:174–180, 2015. doi:10.1016/j.carbon.2015.06.041.

[61] W. Wang and Z. Li. Potential barrier of graphene edges. *Journal of Applied Physics*, 109(11):114308, 2011. doi:10.1063/1.3587186.

[62] R. Whitesides and M. Frenklach. Detailed kinetic Monte Carlo simulations of graphene-edge growth. *The Journal of Physical Chemistry A*, 114(2):689–703, 2010. doi:10.1021/jp906541a.

[63] T. C. Wu, H. J. Hsin, M. Y. Kuo, C. H. Li, and Y. T. Wu. Synthesis and Structural Analysis of a Highly Curved Buckybowl Containing Corannulene and Sumanene Fragments. *Journal of the American Chemical Society*, 133(41):16319–16321, 2011. doi:10.1021/ja2067725.

[64] X. Z. Wu, Y. R. Yao, M. M. Chen, H. R. Tian, J. Xiao, Y. Y. Xu, M. S. Lin, L. Abella, C. B. Tian, C.-L. Gao, Q. Zhang, S. Y. Xie, R. B. Huang, and L. S. Zheng. Formation of Curvature Subunit of Carbon in Combustion. *Journal of the American Chemical Society*, 138(30):9629–9633, 2016. doi:10.1021/jacs.6b04898.

[65] Z. Xu, Z. Liang, and F. Ding. Isomerization of $sp^2$-hybridized carbon nanomaterials: structural transformation and topological defects of fullerene, carbon nanotube, and graphene. *Wiley Interdisciplinary Reviews: Computational Molecular Science*, 7(2): e1283, 2017. doi:10.1002/wcms.1283.

[66] H. Yang, A. J. Mayne, M. Boucherit, G. Comtet, G. Dujardin, and Y. Kuk. Quantum interference channeling at graphene edges. *Nano Letters*, 10(3):943–947, 2010. doi:10.1021/nl9038778.

[67] E. K. Y. Yapp, C. G. Wells, J. Akroyd, S. Mosbach, R. Xu, and M. Kraft. Modelling (PAH) curvature in laminar premixed flames using a detailed population balance model. *Combustion and Flame*, 176:172 – 180, 2017. doi:10.1016/j.combustflame.2016.10.004.

[68] N. Yoshizawa, Y. Yamada, and M. Shiraishi. TEM lattice images and their evaluation by image analysis for activated carbons with disordered microtexture. *Journal of Materials Science*, 33(1):199–206, 1998. doi:10.1023/A:1004322402779.

[69] X. You, R. Whitesides, D. Zubarev, W. A. Lester, and M. Frenklach. Bay-capping reactions: Kinetics and influence on graphene-edge growth. *Proceedings of the Combustion Institute*, 33(1):685–692, 2011. doi:10.1016/j.proci.2010.05.110.

[70] A. V. Zabula, A. S. Filatov, S. N. Spisak, A. Y. Rogachev, and M. A. Petrukhina. A Main Group Metal Sandwich: Five Lithium Cations Jammed Between Two Corannulene Tetraanion Decks. *Science*, 333(6045):1008–1011, 2011. doi:10.1126/science.1208686.

# A Appendix

## A.1 Strained corannulene

Electronic structure calculations were performed on a set of corannulene structures with constrained geometry. The constrained variable was the internal dihedral angle $\phi$ between the pentagonal and the hexagonal rings (as shown in Figure S1). All other coordinates were optimised for geometries of varying $\phi$ ranging from 180° to 140° in 2° increments. Three of the constrained and optimised structures are shown in Figure S1. The total pyramidalisation angle, $\theta_{\text{tot}} = \sum_{C_{\text{hub}}} \theta_p \mathbf{v}_\pi$, was then computed (compare to Eq3). The magnitude of the dipole moment $\mu$ was calculated at the B3LYP/cc-pVQZ level of theory using the Gaussian 09 software [16]. The dependence of $\mu$ on $\theta_{\text{tot}}$ is shown in Figure S1. The linear model Eq 3 is shown for comparison, with slope $f_{\theta_p}$ = 2.24 D/rad, as determined in Figure 5. As seen, the dependence of $\mu$ on $\theta_{\text{tot}}$ shows non-linearity even at rather small values of the angle, and the success of Eq 3 seems to be due to fortuitous cancellation of effects at larger pyramidalisation.

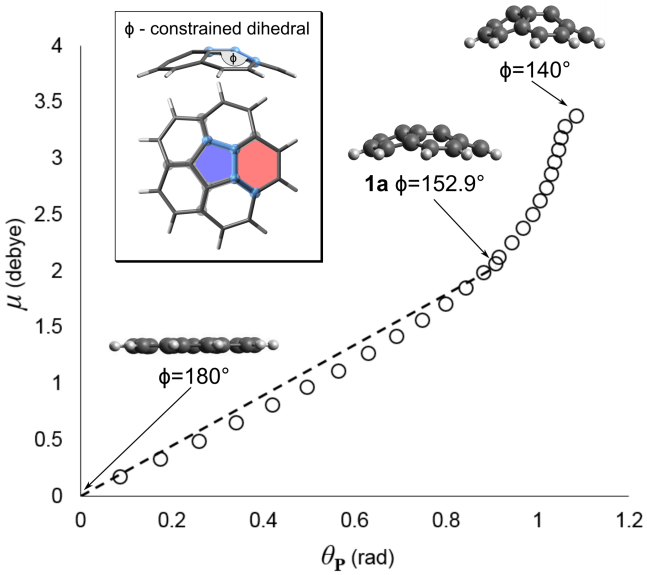


**Figure S1:** *The magnitude of the dipole moment of the strained corannulene geometries are plotted versus the total pyramidalisation angle $\theta_{tot}$. The dihedral angle which is constrained in the geometry optimisation is shown in the boxed inset. Three of the geometries with their corresponding dihedral angles are inset. The dashed line corresponds to Eq 3.*

The ELF of the flat ($\phi$ = 180°) and the relaxed ($\phi$ = 152.9°) corannulene structures are compared in Figure S2. This figure shows clearly the squeezing of electron density to the convex side of the molecule and the resulting greater localisation there.

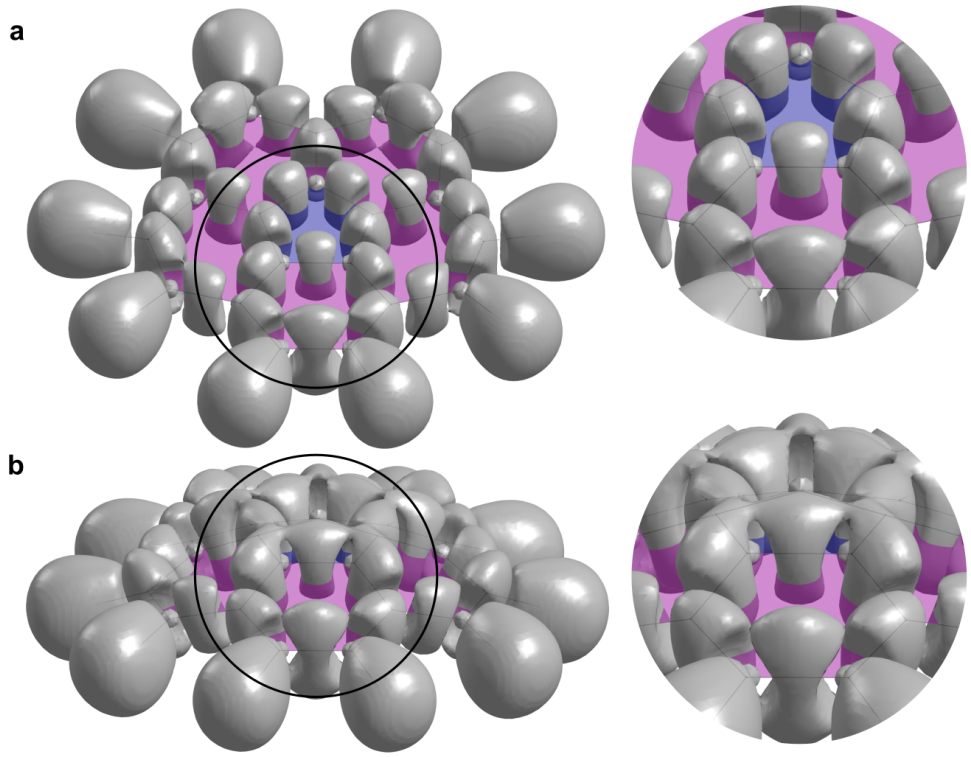


**Figure S2:** *Plot of the iso-surfaces of the electron localisation function for corannulene **1a** at iso=0.66 for a) flattened and b) relaxed corannulene. Insets on the right are expanded views near the π bonding region at the hub showing the asymmetry of the bond.*

## A.2 Distributed multipole expansion

Two methods were employed to determine the atom-centred multipoles: the atoms in molecules (AIM) approach [3] and the Gaussian distributed multipole analysis (GDMA) method [52]. The AIM approach partitions the atoms into volumes with the condition $\nabla\rho(\mathbf{r}) = 0$ defining the interfaces between them, $\rho$ is the electron density. The AIM analysis was performed on corannulene and dicircumcorannulene using the Multiwfn program [35] using a grid spacing of 0.06 Bohr. Figure S3 shows a *xy* cross section through the molecules. The blue lines show the interface of the two atomic volumes in cross section.

By integration of the charge density (electron density along with the nuclei) over the atomic volume, the AIM analysis allows the calculation of the atom-centred multipoles up to quadrupole moments. This method produces reasonable values of the atom-centred multipole moments, which are size extensible and independent of the basis set [36] as the decomposition uses the electron density directly as provided by the electronic structure calculation. However, the partitioning and numerical integration are computationally expensive and could not be applied to the largest carbon structures we study. The GDMA method is of lower computational cost as it provides the atom-centred multipoles directly from the optimised molecular orbital calculations.

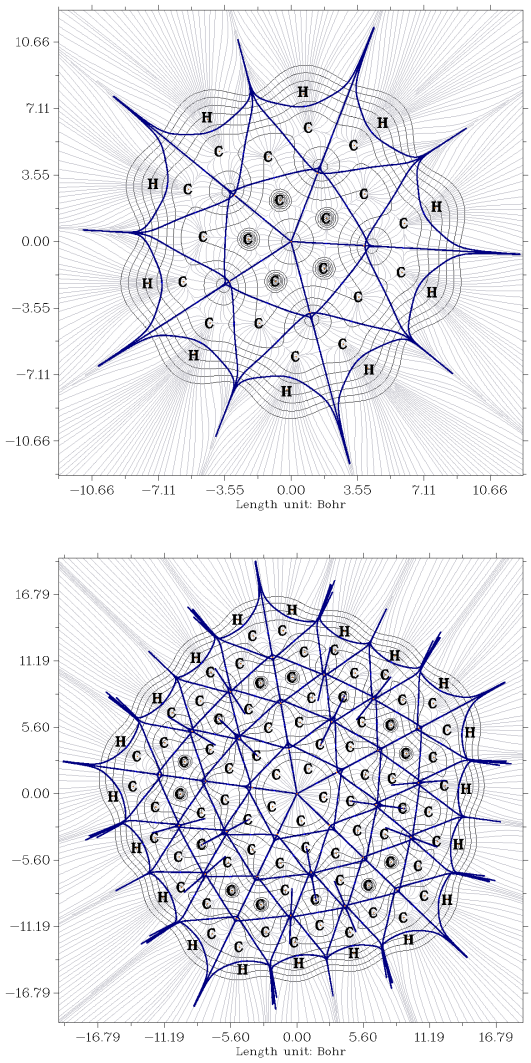


**Figure S3:** *Cross section of the molecular volumes/basins calculated using the atoms in molecules approach for the molecules **1a** and **1b**.*

As the flexoelectric dipole moment has been found in this study to be important, the atom-centered dipoles were compared between the GDMA($C_2H_2$) method and the AIM method as the benchmark. For the molecule corannulene **1a**, the flexoelectric dipoles at the hub of the molecule were of similar magnitude (<10%) and direction for the different decompositions. Figure S4 shows a vector representation of the atomic centered dipole moments for dicircumcorannulene **1b** using two variants of GDMA, where the length is proportional to the magnitude of the moment. The GDMA($C_2H_2$) method produces dipoles at the hub C atoms that are 40-50% larger than the AIM method, Figure S4a. In addition, it produces a very high dipole moment at the hydrogen atoms (in addition to the positive point charge) that has no intuitive physical explanation. The second variant of the Gaussian distributed multipole decomposition, GDMA($C_2H_0$), is with multipole rank at the H atoms set to 0 (point charges only). GDMA($C_2H_0$) compares very well with the "benchmark" AIM multipoles, Figure S4 b and produces intuitively reasonable values of

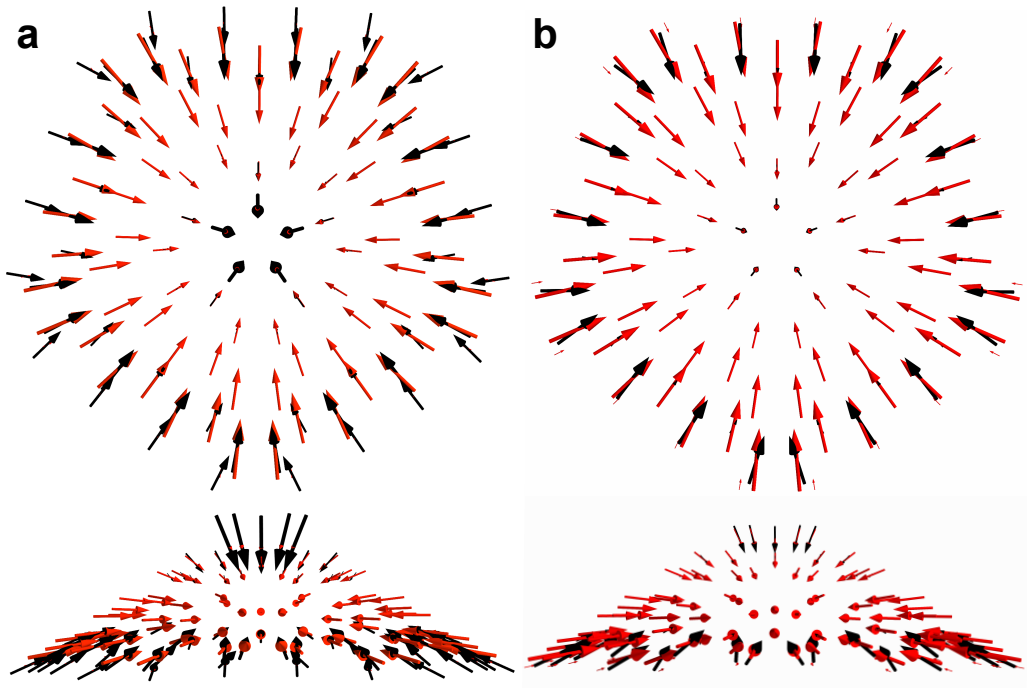


**Figure S4:** *Atom-centred dipole moments plotted as vectors for circum-2-corannulene calculated using the AIM approach (red arrows) and the GDMA method (black arrows). In a, GDMA($C_2H_2$) is shown with rank=2 multipoles on all atoms, hydrogens included. In b, the GDMA($C_2H_0$) dipoles are given, where restricted expansion (rank=0) of the atomic multipoles on the hydrogen atoms is utilised.*

the point charges and dipoles, as discussed in Section 4.